and in fact used five. By utilizing the fine splitting of layer lines due to the imperfect repeat of the TMV helix (Makowski, 1980) and the small differences in splitting among the derivatives, we have solved the same structure using only two derivatives, obtaining an electron density map of comparable quality.

Structures other than TMV often have more Bessel orders contributing to a layer line at a given resolution, and use must be made of all available information to solve their structures. Preparation of heavy-atom derivatives for use in fiber diffraction is difficult, since most fiber structures are unusually sensitive to chemical disturbance [for example, microtubules (Ludueña, 1979)] or have surfaces with a specific protective function (as in viruses) and so are very resistant to modification. Furthermore, location of heavy atoms in a helical structure presents special difficulties (Holmes, Mandelkow & Barrington Leigh, 1972; Holmes *et al.*, 1975). Any method such as the one presented here which increases the information available from each derivative will greatly extend the resolution attainable in structural studies using fiber diffraction.

This work was supported by NIH grants GM25236, CA24407 and CA29522, and by an Alfred P. Sloan Foundation Fellowship to LM.

References

BARRETT, A. N., BARRINGTON LEIGH, J., HOLMES, K. C., LEBERMAN, R., MANDELKOW, E., VON SENGBUSCH, P. & KLUG, A. (1971). *Cold Spring Harbor Symp. Quant. Biol.* **36**, 433–448.

BLOOMER, A. C., CHAMPNESS, J. N., BRICOGNE, G., STADEN, R. & KLUG, A. (1978). *Nature (London)*, **276**, 362–368.

CHAMPNESS, J. N., BLOOMER, A. C., BRICOGNE, G., BUTLER, P. J. G. & KLUG, A. (1976). *Nature (London)*, **259**, 20–24.

COCHRAN, W., CRICK, F. H. C. & VAND, V. (1952). *Acta Cryst.* **5**, 581–586.

FRANKLIN, R. E. & KLUG, A. (1955). *Acta Cryst.* **8**, 777–780.

FRASER, R. D. B., MACRAE, T. P., MILLER, A. & ROWLANDS, R. J. (1976). *J. Appl. Cryst.* **9**, 81–94.

HOLMES, K. C. & BARRINGTON LEIGH, J. (1974). *Acta Cryst.* A**30**, 635–638.

HOLMES, K. C., MANDELKOW, E. & BARRINGTON LEIGH, J. (1972). *Naturwissenschaften*, **59**, 247–254.

HOLMES, K. C., STUBBS, G. J., MANDELKOW, E. & GALLWITZ, U. (1975). *Nature (London)*, **254**, 192–196.

KLUG, A., CRICK, F. H. C. & WYCKOFF, H. W. (1958). *Acta Cryst.* **11**, 199–213.

LUDUEÑA, R. F. (1979). *Microtubules*, edited by K. ROBERTS & J. S. HYAMS. New York: Academic Press.

MAKOWSKI, L. (1978). *J. Appl. Cryst.* **11**, 273–283.

MAKOWSKI, L. (1980). In *Fiber Diffraction Methods*, edited by A. D. FRENCH & K. H. GARDNER. American Chemical Society Symposium Series, Vol. 141, pp. 139–148.

STUBBS, G., WARREN, S. & HOLMES, K. (1977). *Nature (London)*, **267**, 216–221.

STUBBS, G. J. & DIAMOND, R. (1975). *Acta Cryst.* A**31**, 709–718.

TOPPING, J. (1955). *Errors of Observation and Their Treatment*. New York: Reinhold.

WASER, J. (1955). *Acta Cryst.* **8**, 142–150.

Acta Cryst. (1982). A**38**, 425–432

Bragg Diffraction From a Material of Circular Cross Section

BY D. K. SALDIN*

Department of Metallurgy and Science of Materials and Department of Engineering Science, University of Oxford, Oxford, England

(*Received* 10 *October* 1981; *accepted* 22 *January* 1982)

Abstract

The problem of dynamical Bragg diffraction from a set of Bragg planes in a material circular in the diffraction plane is solved by a combination of a Riemann-function technique and numerical integration of the Takagi–Taupin equations. In regions affected by non-Laue surfaces the solution is compared with an approximate Green-function method based on truncation of small arcs of the circle. The bright-field and dark-field intensity profiles are determined only by the radius of the circle compared to the extinction distance, and on the absorption parameters. The dependence of the profiles on these parameters is studied.

* Present address: Blackett Laboratory, Department of Physics, Imperial College of Science and Technology, Prince Consort Road, London SW7, England.

0567-7394/82/040425-08$01.00

1. Introduction

The dynamical theory of X-ray diffraction was first developed for infinitely broad plane waves incident on infinitely broad plane crystal surfaces in both the Bragg case (Darwin, 1914*a*,*b*) and the Laue case (Ewald, 1916*a*,*b*, 1917). In the diffraction of X-rays from a finite crystal, however, it is necessary to consider a problem in which the boundary conditions on the wave amplitudes at the crystal surface vary over the surface, which may be divided into separate regions as follows: If the incident wave impinges on a surface and both the transmitted and diffracted waves propagate into the crystal, the surface is known as a Laue surface, whereas if the diffracted wave emerges from the same surface it is known as a Bragg surface. If a surface is such that the forward propagating wave in the crystal emerges from it, but the Bragg diffracted wave does not, the surface is termed a rear surface. The diffraction problem may be formulated mathematically as that of solving the Takagi–Taupin equations,

$$\frac{\partial \psi_0}{\partial s_0} = i\Gamma_1 \psi_1 \tag{1}$$

$$\frac{\partial \psi_1}{\partial s_1} = i\Gamma_1 \psi_0 \tag{2}$$

subject to the boundary conditions

$$\left.\begin{aligned} \psi_0 &= \Phi_0 \qquad (3)\\ \frac{\partial \psi_1}{\partial s_1} &= i\Gamma_1 \Phi_0 \qquad (4)\end{aligned}\right\} \text{on Bragg surfaces,}$$

$$\left.\begin{aligned} \psi_0 &= \Phi_0 \qquad (5)\\ \psi_1 &= 0 \qquad (6)\end{aligned}\right\} \text{on Laue surfaces}$$

and

$$\left.\begin{aligned} \psi_1 &= 0 \qquad (7)\\ \frac{\partial \psi_0}{\partial s_0} &= 0 \qquad (8)\end{aligned}\right\} \text{on rear surfaces,}$$

where ψ_0 and ψ_1 are the amplitudes of the forward-propagating (bright-field) and diffracted (dark-field) beams, s_0 and s_1 are coordinates in the directions of propagation of the crystal waves and Γ_1 is a coupling coefficient defined by

$$\Gamma_1 = -\pi |\mathbf{K}| C \chi_1. \tag{9}$$

In (9), $\mathbf{K}$ represents the wave vector of the plane wave incident on the crystal, χ_1 is the first-order Fourier coefficient of the crystal polarizability and C is the polarization factor, which for electromagnetic waves is unity when the electric-field vector is perpendicular to the diffraction plane and is equal to $\cos 2\theta_B$ when it lies in the plane (θ_B is the Bragg angle). The quantity Φ_0 is defined by

$$\Phi_0 = \Psi_0 \exp(-2\pi i[\mathbf{K} - \mathbf{k}_0].\mathbf{r}_e), \tag{10}$$

where Ψ_0 is the amplitude of the incident plane wave, $\mathbf{k}_0$ is the wave vector of the forward-propagating crystal wave (making an angle θ_B with the Bragg planes) and $\mathbf{r}_e$ is a position vector on the wave-input surface.

The most elegant solution of this problem is by writing (1) and (2) as telegraphy equations,

$$\frac{\partial^2 \psi_i}{\partial s_0 \, \partial s_1} + \Gamma_1^2 \psi_i = 0, \quad \text{where } i = 0, 1, \tag{11}$$

and by use of Riemann- (or Green-) function techniques. The diffracted beam amplitude at any point P in the crystal depends only on diffraction processes within a domain of dependence or Takagi fan (Takagi, 1969). The form of the Green function depends on the nature of the crystal surface intersecting the Takagi fan. When this is purely a Laue surface, Takagi (1969) pointed out that the Green function is the standard Riemann function well known in the theory of the telegraphy equation (Courant & Hilbert, 1966) and the form of this function is independent of the shape of the surface.

A very useful extension of this theory for the case where the crystal surface intersecting the Takagi fan may consist partly of Bragg and rear surfaces was discovered by Uragami (1971). Defining Green functions v_i ($i = 0, 1$) satisfying the (self-)adjoint equation

$$\frac{\partial^2 v_i}{\partial s_0 \, \partial s_1} + \Gamma_1^2 v_i = 0, \tag{12}$$

subject to the boundary conditions

$$v_0 = v_1 = 1 \tag{13}$$

on the lines through P parallel to the s_0 and s_1 axes,

$$v_0 = 0, \quad \frac{\partial v_1}{\partial s_0} = 0 \tag{14}$$

on Bragg surfaces, and

$$\frac{\partial v_0}{\partial s_1} = 0, \quad v_1 = 0 \tag{15}$$

on rear surfaces within the Takagi fan, Uragami (1971) showed that it is possible to find expressions for $\psi_0(P)$ and $\psi_1(P)$ in terms of these functions.* Uragami (1971) further went on to give explicit forms for the v_i when the Bragg and rear surfaces are planar. The validity of this solution was confirmed by the work of Saka, Katagawa & Kato (1972*a*,*b*, 1973) who used a method based on the Fourier decomposition of crystal waves. When the Bragg and rear surfaces are not planar, however, no

* It will be noted that, unlike the situation in the purely Laue case, the Green functions v_i depend on the shapes of the Bragg and rear surfaces *via* the additional boundary conditions (14) and (15).

Green functions have yet been found satisfying conditions (14) and (15).

A form of finite crystal of great interest due to its frequent natural occurrence is the cylinder.

An approximate solution of the diffraction problem in this case has been given by Saldin & Buckley-Golder (1977) and Olekhnovich & Olekhnovich (1980), based on replacing small curved regions of Bragg and rear surfaces by planes.

It is clear of course that for large Bragg angles this approximation is unlikely to be valid. However, it is of interest whether the approximation is reasonable for relatively small Bragg angles. In the computations of this paper we have taken the value of $\theta_B = 9{\cdot}8°$ appropriate to the case of Mo $K\alpha_1$ X-rays diffracted by (111) planes in copper. Calculations were performed of the bright- and dark-field intensity distributions from a cylindrical crystal of copper with the (111) diffracting planes parallel to the axis of the cylinder. Two methods were used; one the Green-function technique, which is exact when the wave-entrant surface is purely of Laue type, and approximate otherwise; the other was based on the numerical solution of the Takagi–Taupin equations for the amplitudes affected by the Bragg and rear surfaces. The approximate Green-function method (for Bragg and rear surfaces) was attempted only for dark field. Absorption was incorporated by allowing χ_0 and χ_1, the zero and first-order Fourier coefficients of the polarizability, to become complex.

2. The Green-function method

The geometry of the diffraction problem is illustrated in Fig. 1, which represents the cross section perpendicular to the axis of a cylindrical crystal. We consider the incidence of a plane wave of infinite width with wave vector **K** making a Bragg angle θ_B (in this paper we restrict ourselves to the case of $\theta_B < 30°$) with a set of crystal planes parallel to the axis of the cylinder. Bragg-diffracted waves with wave vectors $\mathbf{k}_0$ and $\mathbf{k}_1$ will be generated. It is clear from the geometry of the figure that the incident wave enters the crystal at all points on the semicircle $R \ldots A_m \ldots T_0$ ($m = 1, \ldots, 5$) while the diffracted wave leaves the crystal at all points on the semicircle $R_0 \ldots P_n \ldots T$ ($n = 1, \ldots, 4$). The forward propagating wave emerges from the crystal on the semicircle $T_0 \ldots P_n \ldots R$. In Uragami's (1971) nomenclature, the arc R_0R would be a Bragg surface, T_0R_0 a Laue surface and TT_0 a rear surface.

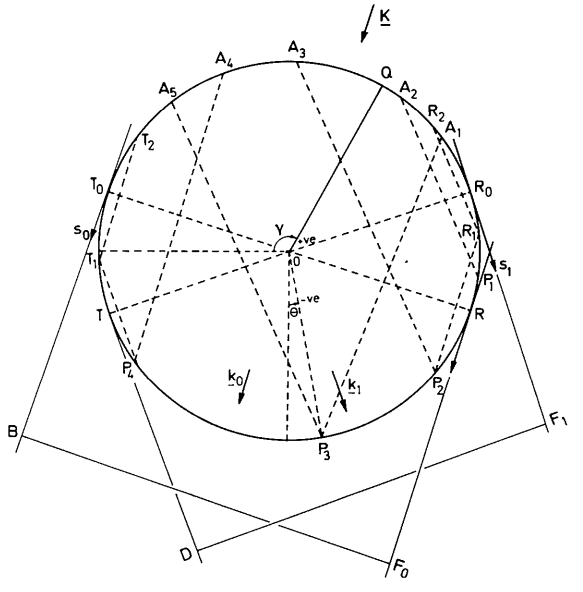

Fig. 1. Cross section of the cylindrical crystal. The diffraction geometry.

If 0 denotes the position of the axis of the cylinder and P_n the position of an arbitrary point on the wave-exit surface, let $0P_n$ make an angle θ with the Bragg planes. Then we need consider separately four ranges for P_n characterized by the index n (= 1, ..., 4) and defined by the following:

$$n = 1: -\pi/2 - \theta_B < \theta \leq -\pi/2 + \theta_B \tag{16}$$

$$n = 2: -\pi/2 + \theta_B < \theta \leq -\pi/2 + 3\theta_B \tag{17}$$

$$n = 3: -\pi/2 + 3\theta_B < \theta \leq \pi/2 - 3\theta_B \tag{18}$$

$$n = 4: \pi/2 - 3\theta_B < \theta \leq \pi/2 - \theta_B. \tag{19}$$

The need to satisfy different combinations of the boundary conditions (3) to (8) and (13) to (15) in each of these regions leads to different expressions for $\psi_0(P_n)$ and $\psi_1(P_n)$ in each case. For simplicity the equations quoted below are for a non-absorbing crystal. Absorption may be incorporated by allowing χ_0, χ_1, Γ_0, Γ_1, $\mathbf{k}_0$ and $\mathbf{k}_1$ to become complex. If we allow the extra subscripts r and i to denote the real and imaginary parts respectively of these quantities it can be shown that (see *e.g.* Takagi, 1969),

$$|\mathbf{K} - \mathbf{k}_{0,r}| = -\chi_{0,r}K/2 \tag{20}$$

and that $\mathbf{k}_{0,i}$ ($= \mathbf{k}_{g,i}$) is a vector in the direction of the Bragg planes. When absorption is present the quantity $\Phi_0(\gamma)$ in the expressions below takes the form

$$\Phi_0(\gamma) = \exp\left\{ i\pi|\chi_{0,r}|Kr\cos(\pi/2 - \theta_B + \gamma) - \ldots \right.$$
$$\left. - \left[\frac{-\pi|\chi_{0,i}|Kr}{\cos\theta_B}\cos(\pi/2 + \gamma) + \frac{\pi|\chi_{0,i}|}{\cos\theta_B}Kr\cos\theta \right] \right\}, \tag{21}$$

where γ is the angular coordinate defined in Fig. 1 and r is the radius of the cylinder.

(A) Region n = 3

This is the simplest of the cases, where we have Laue-case diffraction and the wave amlitudes at P_3 are given in terms of the Riemann functions,

$$v_0 = v_1 = w_1^K = w_0^K = J_0[\alpha(S_0^K S_1^K)^{1/2}], \tag{22}$$

where

$$\alpha = -2\Gamma_1, \quad S_0^K = s_0^0 - s_1, \quad S_1^K = s_1^0 - s_1, \tag{23}$$

and J_0 is the zero-order Bessel function (see *e.g.* Courant & Hilbert, 1966; Takagi, 1969; Uragami, 1971).

The expressions for the amplitudes are

$$\psi_0(P_3) = \Phi_0(A_1) - \int_{\gamma(A_5)}^{\gamma(A_1)} \frac{\partial v_0}{\partial s_1} \Phi_0(\gamma) \times \cos(\pi/2 + \theta_B - \gamma)\, r\, \mathrm{d}\gamma \tag{24}$$

$$\psi_1(P_3) = \Gamma_1 \int_{\gamma(A_5)}^{\gamma(A_1)} v_1\, \Phi_0(\gamma) \times \cos(\pi/2 + \theta_B - \gamma)\, r\, \mathrm{d}\gamma. \tag{25}$$

The coordinates of P_n are (s_0^0, s_1^0) and those of the general point Q which lies on the cylindrical wave-input surface between A_1 and A_5 are (s_0, s_1). If the origin of the coordinates is defined to be at R_0, we may write

$$\begin{aligned} s_0^0 &= r\{\sin(\theta + \theta_B) + 1\}/\sin 2\theta_B, \\ s_1^0 &= r\{\sin(\theta_B - \theta) - \cos 2\theta_B\}/\sin 2\theta_B \end{aligned} \tag{26}$$

$$\begin{aligned} s_0 &= r\{\cos(\gamma + \theta_B) + 1\}/\sin 2\theta_B, \\ s_1 &= -r\{\cos(\theta_B - \gamma) - \cos 2\theta_B\}/\sin 2\theta_B. \end{aligned} \tag{27}$$

Then

$$\gamma(A_1) = \pi/2 - \theta + 2\theta_B \tag{28}$$

$$\gamma(A_5) = \pi/2 - \theta - 2\theta_B \tag{29}$$

$$\Phi_0(\gamma) = \exp\{-i\Gamma_0 r \cos(\pi/2 - \theta_B + \gamma)\}, \tag{30}$$

where

$$\Gamma_0 = \pi K C \chi_0. \tag{31}$$

(B) Region n = 4

In the calculation of the diffracted-beam amplitude at P_4 we notice that the part $T_0 A_4$ of the crystal surface within the Takagi fan is a Laue surface and the part $T_1 T_0$ is a rear surface. If we replace the arc $T_1 T_0$ by the chord $T_1 T_0$, we find that the Green function v_1 satisfying the boundary conditions (13) to (15) is the composite one consisting of the function w_1^K of (18) in the region $T_1 T_2 A_4 P_4$ and the function

$$v_1 = w_1^K + w_1^{BK}, \tag{32}$$

where

$$w_1^{BK} = -J_0[\alpha(S_0^{BK} S_1^{BK})^{1/2}] \tag{33}$$

$$S_0^{BK} = \mathscr{R}_0 s_0^0 + s_1^{b1} - s_1 \tag{34}$$

$$S_1^{BK} = \mathscr{R}_1 s_1^0 + s_0^{b1} - s_0 \tag{35}$$

$$\mathscr{R}_0 = 1/\mathscr{R}_1 = \frac{\sin(-\pi/4 + 3\theta_B/2 + \theta/2)}{\sin(\theta_B/2 - \pi/4 - \theta/2)} \tag{36}$$

$$s_0^{b1} = \frac{2r\cos\theta_B \sin\{\frac{1}{2}(3\pi/2 - \theta_B - \theta)\}}{\sin\{\frac{1}{2}(-\pi/2 + 3\theta_B + \theta)\}} \tag{37}$$

$$s_1^{b1} = \frac{-2r\cos\theta_B \sin\{\pi/4 + \theta_B/2 + \theta/2\}}{\sin\{\pi/4 + \theta_B/2 - \theta/2\}} \tag{38}$$

in the region $T_1 T_0 T_2$. ($T_2 T_1$ is in the direction of the s_0 axis.) We may write

$$\psi_1(P_4) = \Gamma_1 \left\{ \int_{\gamma(T_2)}^{\gamma(A_4)} w_1^K + \int_{\gamma(T_0)}^{\gamma(T_2)} (w_1^K + w_1^{BK}) \right\} \times \Phi_0(\gamma) \cos(\pi/2 + \theta_B - \gamma)\, r\, \mathrm{d}\gamma, \tag{39}$$

where

$$\gamma(T_0) = \theta_B \tag{40}$$

$$\gamma(T_2) = -\pi/2 + 4\theta_B + \theta \tag{41}$$

$$\gamma(A_4) = \pi/2 - \theta + 2\theta_B. \tag{42}$$

Equation (39) differs from the corresponding expression given by Olekhnovitch & Olekhnovitch (1980) which appears to contain only the Green function w_1^{BK}. Their Green function does not satisfy the relevant one of the boundary conditions (15).

(C) Region n = 1

The point P_1 lies on a Bragg surface and the wave-input surfaces within its Takagi fan consist of a Laue surface $A_2 R_0$ and a Bragg surface $R_0 P_1$. If we replace the arc $R_0 P_1$ by the chord $R_0 P_1$, v_1 becomes Uragami's Green function corresponding to a planar Bragg surface $R_0 P_1$ and may in this case be written

$$v_1 = w_1^{F1U} = \xi_0 \frac{S_0^K}{S_1^K} J_2[\alpha(S_0^K S_1^K)^{1/2}], \tag{43}$$

where $\alpha = -2\Gamma_1$, J_2 is the second-order Bessel function, and

$$\xi_0 = 1/\xi_1 = \frac{\sin(-\pi/4 + 3\theta_B/2 - \theta/2)}{\sin(\theta_B/2 + \pi/4 + \theta/2)}. \tag{44}$$

We may then write

$$\psi_1(P_1) = \Gamma_1 \int_{\gamma(A_2)}^{(R_0)} v_1\, \Phi_0(\gamma) \cos(\pi/2 + \theta_B - \gamma)\, r\, \mathrm{d}\gamma + \int_{s_1(R_0)}^{s_1(P_1)} v_1\, \Phi_0(s_1)\, \mathrm{d}s_1, \tag{45}$$

where the integral over the Laue surface is performed over the angular coordinate γ and that over the Bragg surface with the linear coordinate s_1. In (28),

$$\gamma(R_0) = \pi - \theta_B \tag{46}$$

$$\gamma(A_2) = \pi/2 - \theta - 2\theta_B \tag{47}$$

$$s_1(P_1) = r\{\sin(\theta_B - \theta) - \cos 2\theta_B\}/\sin 2\theta_B \tag{48}$$

$$s_1(R_0) = 0 \tag{49}$$

$$\Phi_0(s_1) = \exp\{\pi i \chi_0 K[-r \sin 2\theta_B + s_1(\xi_1 + \cos 2\theta_B)]\}. \tag{50}$$

(*D*) *Region* $n = 2$

In the case of the point P_2 we see that the crystal surfaces within the corresponding Takagi fan consist of a Laue surface A_3R_0 and a Bragg surface R_0R_1. If we replace the arc R_0R_1 by the chord R_0R_1, then we find that the Green function v_1 satisfying the boundary conditions (16) and (17) is the composite function $v_1 = w_1^K$ in the region $R_1R_2A_3P_2$ and the function

$$v_1 = w_1^K + w_1^{F1U} \tag{51}$$

in the region $R_1R_0R_2$, where

$$w_1^{F1U} = \xi_0 \frac{S_1^{F1U}}{S_0^{F1U}} J_2[\alpha(S_0^{F1U} S_1^{F1U})^{1/2}] \tag{52}$$

$$S_0^{F1U} = \xi_0 s_1^0 - s_1 \tag{53}$$

$$S_1^{F1U} = \xi_1 s_1^0 - s_0 \tag{54}$$

$$\xi_0 = 1/\xi_1 = \frac{\sin(\pi/4 + \theta_B/2 + \theta/2)}{\sin(3\theta_B/2 - \pi/4 - \theta/2)}. \tag{55}$$

We may then write

$$\psi_1(P_2) = \Gamma_1 \left\{ \int_{\gamma(A_3)}^{\gamma(R_2)} w_1^K + \int_{\gamma(R_2)}^{\gamma(R_0)} (w_1^K + w_1^{F1U}) \right\} \times \Phi_0(\gamma) \cos(\pi/2 + \theta_B - \gamma)\, r\, d\gamma + \Gamma_1 \int_{s_1(R_1)}^{s_1(R_0)} (w_1^K + w_1^{F1U})\, \Phi_0(s_1)\, ds_1, \tag{56}$$

where

$$\gamma(A_3) = \pi/2 - \theta - 2\theta_B \tag{57}$$

$$\gamma(R_2) = 3\pi/2 - 4\theta_B + \theta \tag{58}$$

$$\gamma(R_0) = \pi - \theta_B \tag{59}$$

$$s_1(R_0) = 0 \tag{60}$$

$$s_1(R_1) = r\{\sin(\theta_B - \theta) - \cos 2\theta_B\}/\sin 2\theta_B. \tag{61}$$

Expression (56) also differs from the corresponding one of Olekhnovitch & Olekhnovitch (1980), whose Green function w_1^{F1U} does not satisfy the relevant one of the boundary conditions (14).

3. Direct numerical solution of Takagi–Taupin equations

The calculation of the diffracted-beam amplitudes by the Green-function method described above has the advantage that the beam amplitudes are given in terms of line integrals over the wave-input surfaces within the relevant Takagi fan. In the case of a crystal for which any Bragg or rear surfaces are curved, however, this method has the disadvantage that it is necessary to truncate the curved surfaces to produce planar ones so as to enable the use of Uragami's (1971) Green functions. In order to overcome this difficulty and to investigate the validity of this approximation, the diffracted-beam amplitudes in regions $n = 1$, 2 and 4 on the wave-exit surface were computed by direct numerical integration of the Takagi–Taupin equations over regions of the crystal affected by the Bragg and rear surfaces. These regions are shown in Fig. 2 as cross-hatched by a uniform grid of intersecting characteristic lines parallel to the s_0 and s_1 axes. The Takagi–Taupin equations,

$$\frac{\partial \psi_0}{\partial s_0} + \Gamma_{0i}\psi_0 = (-\Gamma_{1i} + i\Gamma_{1r})\psi_1 \tag{62}$$

$$\frac{\partial \psi_1}{\partial s_1} + \Gamma_{0i}\psi_0 = (-\Gamma_{1i} + i\Gamma_{1r})\psi_0, \tag{63}$$

were replaced by the finite difference equations,

$$\frac{\psi_0^C - \psi_0^B}{\Delta} + \Gamma_{0i}\frac{(\psi_0^C + \psi_0^B)}{2} = (-\Gamma_{1i} + i\Gamma_{1r})\frac{(\psi_1^B + \psi_1^C)}{2} \tag{64}$$

$$\frac{\psi_1^C - \psi_1^A}{\Delta} + \Gamma_{0i}\frac{(\psi_1^C + \psi_1^A)}{2} = (-\Gamma_{1i} + i\Gamma_{1r})\frac{(\psi_0^A + \psi_0^C)}{2}, \tag{65}$$

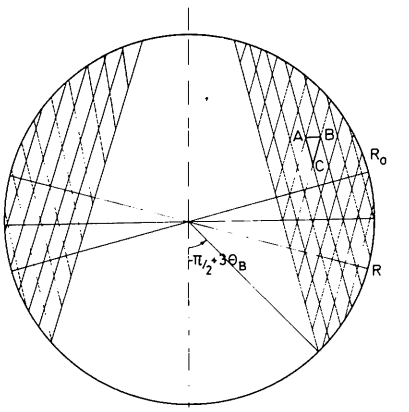

Fig. 2. Integration mesh used in numerical solution of Takagi–Taupin equations.

relating the beam amplitudes at typical neighbouring points A, B and C at the vertices of an element of the grid when A, B and C are all within the bulk of the crystal ($\Delta = AC = BC$). Thus knowledge of the beam amplitudes at A and B enable those at C to be determined and the beam amplitudes throughout the cross-hatched regions may be found. Modifications to (60) and (61) are needed only when a crystal surface intersects two of the sides of the triangle ABC. These cases are illustrated in Fig. 3:

Case (a): Surface intersecting AC and BC

In this case the point C is assumed to lie on a Laue surface. The beam amplitudes at C are assigned the values $\psi_0^C = \Phi_0$ and $\psi_1^C = 0$.

Case (b): Surface intersecting AB and BC

This can happen when the intersecting surface is either Laue or Bragg and we take $\psi_0^C = \Phi_0$ and ψ_1^C is evaluated from (64).

Case (c): Surface intersecting AB and AC

In this case the intersecting surface is either a Laue or a rear surface and we assign $\psi_1^C = 0$ and evaluate ψ_0^C from (65).

4. Results of the calculations

Shown in Fig. 4 are the calculated intensity profiles, for a range of diameters of crystal, expected on a film placed along BF_0 (bright field) and DF_1 (dark field) in Fig. 1. If one imagines an X-ray topography experiment, the intensity profiles along BF_0 and DF_1 represent the bright- and dark-field section topographs expected from a wide coherent X-ray beam incident over the whole of the cross section of the cylinder. The calculations giving rise to the profiles of Fig. 4 assume no absorption and in this case the form of the profiles depends only on the value of the parameter $N = \Gamma_1 d/\pi$, where d ($= 2r$) is the diameter of the cylinder, and on the size of the Bragg angle θ_B (which here is assumed to be 0·171 rad). When N is equal to an integer, d is equal to a whole number of extinction distances and when this quantity is half-integral d is equal to an odd number of half-extinction distances.

The bright-field intensities are high near the centre of the profile in the former case and low in the latter case. The converse behaviour is found for the dark-field profiles, indicating a *Pendellosung*-type oscillation of intensities between the coupled beams for the parts of the profile determined essentially by Laue-case diffraction. The solid curves represent the results of the more accurate calculations (*i.e.* those using the Riemann-function method for Laue-case diffraction and the numerical solution of the Takagi–Taupin equations for Bragg-case and rear-surface diffraction). Where they deviate from these profiles the dotted curves are the result of the approximate Green-function calculation for dark-field intensities affected by Bragg-case and rear-surface diffraction.

The two curves are virtually coincident for rear-surface diffraction but deviate greatly for Bragg-case diffraction for $N \gtrsim \frac{1}{2}$. Both curves predict a peak in the dark-field profiles for intensities affected by Bragg-case diffraction, and this is not unexpected since it is known that when the Bragg surface is planar and infinite all of

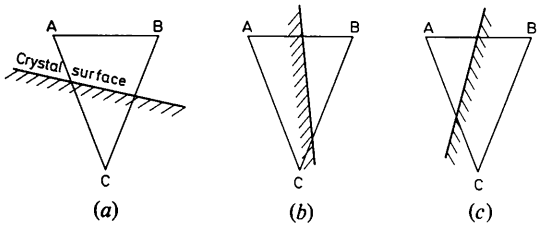

Fig. 3. Intersection of the crystal surfaces with various elements of characteristic mesh.

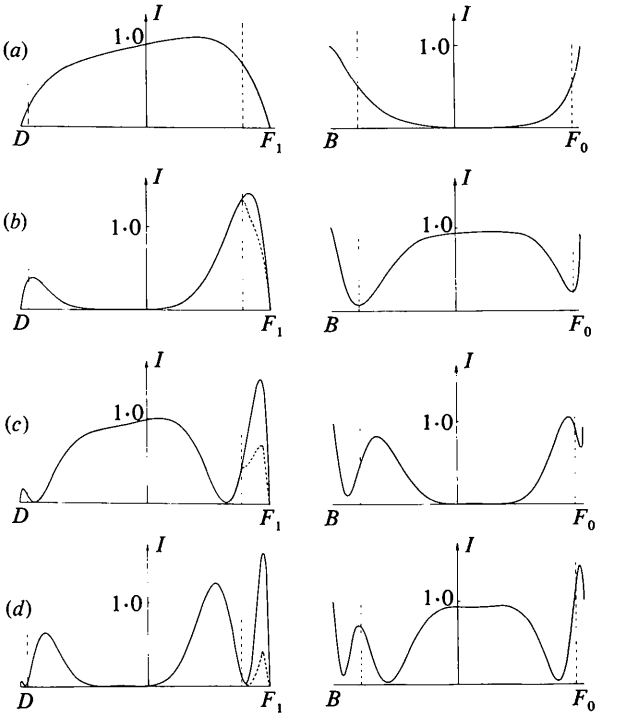

Fig. 4. Intensity profiles due to diffraction from cylinder. Shown are dark-field profiles (along DF_1) and bright-field (along BF_0). The vertical dotted lines separate intensities determined by pure Laue-case diffraction from those affected by non-Laue edges. In the latter case the solid profiles depict the numerical solution and the dotted profiles the approximate Green-function solutions. Zero absorption. Unit incident intensity. (*a*) $N = \frac{1}{2}$, (*b*) $N = 1$, (*c*) $N = 1\frac{1}{2}$, (*d*) $N = 2$.

the incident power is transferred to the diffracted beam. The height of the peak predicted by the numerical solution is considerably greater than that of the approximate Green function solution. A further point of interest is that for $N = 2$ the bright-field profile also acquires a narrow peak near F_0. Both Bragg peaks may acquire intensities greater than that of the incident beam. However, the sum of the areas under the bright- and dark-field profiles (solid lines) is constant, independent of the value of N, and equal to the area under the incident beam's (flat) profile, thus confirming power conservation for this no-absorption diffraction process.

The absence of a Bragg peak in the profile with the lowest value of N indicates a beginning of a transition to the regime of kinematical diffraction, where there is no important distinction between the Laue and Bragg cases, and where the dark-field amplitude at any point is proportional to the path length of the diffracted beam in the material. Indeed, for lower values of N the dark-field profiles (not shown) bore out this prediction quite well, and were symmetric about the I axis.

The effect of absorption (both normal and 'anomalous') on these profiles is illustrated in Fig. 5. The main effect is to flatten out the profiles (*i.e.* to reduce the peaks and elevate the dips in the profile). The latter consequence is of course due to 'anomalous' absorption (or transmission), that is, essentially the Borrmann effect. The absorption parameters used were those appropriate to (111) diffraction of Mo $K\alpha_1$ radiation (of wavelength 0·0709 nm) from a copper crystal (*i.e.* the ratio Γ_{0i}/Γ_{1r} was taken to be 0·0567 and it was assumed that $\Gamma_{1i} = \Gamma_{0i}$).

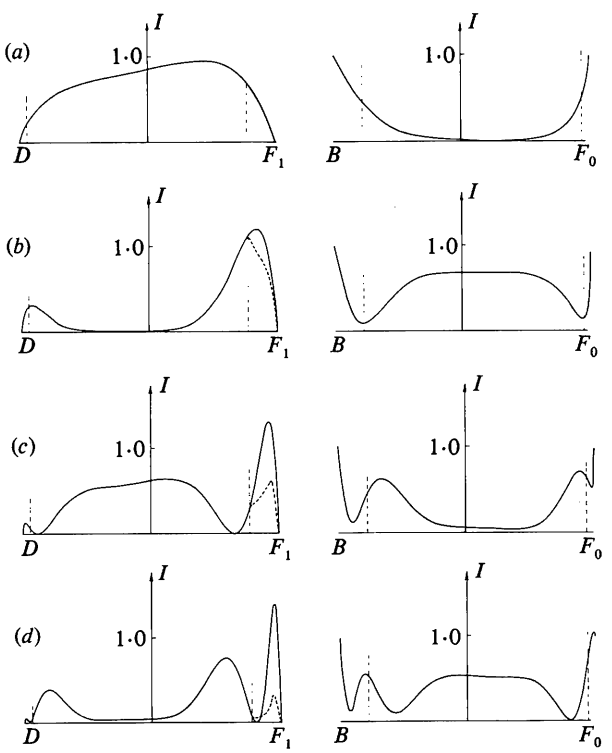

Fig. 5. Same as Fig. 4 except that the calculations were for an absorbing crystal with $\Gamma_{0i}/\Gamma_{1r} = 0{\cdot}0567$ and $\Gamma_{1i} = \Gamma_{0i}$.

The shapes of the profiles for larger values of N are illustrated in Fig. 6. Shown here are bright- and dark-field profiles for $N = 4$ and 4·5. Absorption was included in the calculations. As may be expected, several fringes are present in the profiles, especially towards the edges. The Bragg peaks appear to consist of a broad envelope containing several narrow fringes. The intensities near the centres of the profiles are similar for bright and dark fields and are also relatively insensitive to the value of N as this quantity is varied by an integer. These results are of course expected as a consequence of 'anomalous' absorption. For large values of N it is no longer necessarily the case that the bright-field intensity is high for integral N and that the dark-field intensity is high for half-integral N. This is due to the large range of lengths of diffraction paths (relative to an extinction length) within the relevant Takagi fan.

5. Conclusions

When a broad beam of coherent radiation is diffracted from a set of Bragg planes in a material with circular cross section in the diffraction plane the bright- and dark-field intensity profiles depend on the size of the circle relative to the extinction distance. When the diameter (d) of the circle is significantly less than half an extinction distance, ξ_1, the features of the bright- and dark-field profiles are in broad agreement with the predictions of the kinematical theory. When $d \gtrsim \frac{1}{2}\xi_1$, however, the dynamical theory predicts a significant

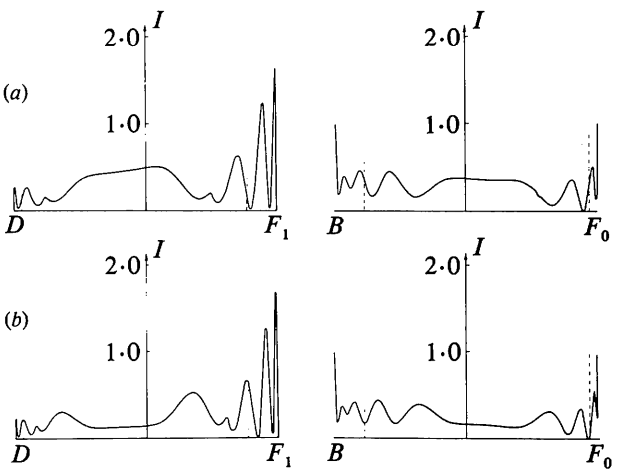

Fig. 6. Intensity profiles for (*a*) $N = 4$ and (*b*) $N = 4\frac{1}{2}$. Absorption parameters as in caption of Fig. 5. The curves show results only from the numerical integration of the Takagi–Taupin equations.

difference between Laue-case and Bragg-case diffraction. Rays affected by the Bragg surface give rise to a high-intensity region on dark-field profiles. The profiles of this peak are *not* well predicted by an approximate Green-function method based on truncated planar Bragg surfaces. As d increases so as to be much greater than about ξ_1, the Bragg peak begins to consist of several narrowly-spaced fringes contained within a broad envelope.

There is some experimental evidence for the presence of such Bragg peaks on X-ray topographs of cylindrical crystals (see *e.g.* Saldin & Buckley-Golder, 1977). In the instance cited above the diameter was of the order of a hundred extinction distances. The narrow Bragg fringes expected were smeared out to form a wide high-intensity region near F_1 on the photographs in this case since they were projection (or traverse) topographs. One method of computing the form of such peaks would be by means of an extension of our calculations and the use of the reciprocity theorem (Kato, 1968).

The author wishes to thank Drs I. M. Buckley-Golder and M. J. Whelan FRS for introducing him to the problem, and Dr P. St J. Russell and Dr L. Solymar for helpful discussions.

References

COURANT, R. & HILBERT, D. (1966). *Methods of Mathematical Physics*, Vol. II, p. 449. New York: Interscience.
DARWIN, C. G. (1914*a*). *Philos. Mag.* **27**, 315–333.
DARWIN, C. G. (1914*b*). *Philos. Mag.* **27**, 675–690.
EWALD, P. P. (1916*a*). *Ann. Phys. (Leipzig)*, **49**, 1–38.
EWALD, P. P. (1916*b*). *Ann. Phys. (Leipzig)*, **49**, 117–143.
EWALD, P. P. (1917). *Ann. Phys. (Leipzig)*, **54**, 519–597.
KATO, N. (1968). *Acta Cryst.* A**24**, 157–160.
OLEKHNOVICH, N. M. & OLEKHNOVICH, A. I. (1980). *Acta Cryst.* A**36**, 22–27.
SAKA, T., KATAGAWA, T. & KATO, N. (1972*a*). *Acta Cryst.* A**28**, 102–113.
SAKA, T., KATAGAWA, T. & KATO, N. (1972*b*). *Acta Cryst.* A**28**, 113–120.
SAKA, T., KATAGAWA, T. & KATO, N. (1973). *Acta Cryst.* A**29**, 192–200.
SALDIN, D. K. & BUCKLEY-GOLDER, I. M. (1977). *Abstracts B, 4th European Crystallographic Meeting*, p. 637. Oxford: Cotswold Press.
TAKAGI, S. (1969). *J. Phys. Soc. Jpn*, **27**, 1239–1253.
URAGAMI, T. S. (1971). *J. Phys. Soc. Jpn*, **31**, 1141–1161.

Acta Cryst. (1982). A**38**, 432–438

On the Evaluation of Root-Mean-Square Errors in Atomic Coordinates in Protein Crystallography

BY Z. S. DEREWENDA, A. M. BRZOZOWSKI, A. STĘPIEŃ AND M. J. GRABOWSKI

Department of Crystallography, Institute of Chemistry, University of Łódź, 91 416 *Łódź, Nowotki* 16, *Poland*

(*Received* 20 *April* 1980; *accepted* 25 *January* 1982)

Abstract

The calculation of standard deviations for atomic coordinates in human deoxyhaemoglobin A on the basis of various reciprocal-space residuals has shown the resulting values to be in good agreement with each other. Evidence is presented that such calculations may be more reliable than is commonly accepted. It is also shown that Wilson's statistics may be applied successfully to low- and high-angle protein diffraction data.

Introduction

It is usually assumed that the calculation of standard deviations of atomic coordinates in a model of a protein molecule is rather difficult. However, the knowledge of its value may prove very helpful, for example in estimating the credibility of the orientation of a known protein molecule in an unknown crystal lattice, found using various molecular replacement techniques.

It is interesting that various reciprocal-space residuals may serve both as correlation functions in rotation and translation function searches (Nixon & North, 1976) and as a basis of $|\overline{\Delta r}|$ evaluation (Luzzati, 1952; Parthasarathy & Parthasarathi, 1972; Nixon & North, 1976). Attention has also been paid to the physical interpretation of refinement based on the minimization of some of these residuals (Wilson, 1976).

On the other hand, the search for the correct orientation of a protein molecule with the molecular replacement method was frequently based on a strictly mathematical assumption that a unique set of correct values of rotational and translational parameters

0567-7394/82/040432-07$01.00